Наносистеми, наноматеріали, нанотехнології
Nanosistemi, Nanomateriali, Nanotehnologii
2025, т. 23, № 1, сс. 135–148
https://doi.org/10.15407/nnn.23.01.0135

PACS numbers: 61.05.cp, 68.37.Og, 72.80.Tm, 77.22.Gm, 78.20.Ci, 78.40.Ri, 81.05.U-

Synthesis, Structure and Electromagnetic Properties of Composite Materials Based on Carbon Nanospheres

O. D. Rud[1], L. Yu. Matsui[2], L. L. Vovchenko[2], I. M. Kirian[1], M. O. Rud[1], A. M. Lakhnyk[1], Yu. V. Lepeeva[1], A. P. Naumenko[2], O. S. Yakovenko[2], Ya. Ye. Pazdriy[3], and D. V. Vinnychenko[4]

[1]*G. V. Kurdyumov Institute for Metal Physics, N.A.S. of Ukraine, 36, Academician Vernadsky Blvd., UA-03142 Kyiv, Ukraine*
[2]*Taras Shevchenko National University of Kyiv, 64/13, Volodymyrska Str., UA-01601 Kyiv, Ukraine*
[3]*Quantum Satis Engineering, 1201, N. Orange Str., 19801 Wilmington, U.S.A.*
[4]*Institute of Electrodynamics, N.A.S. of Ukraine,. 56, Beresteiskyi Ave., UA-03057 Kyiv, Ukraine*

The influence of carbon nanospheres (CNS) on the electromagnetic properties of composite materials is investigated. CNS are fabricated by high-frequency electrical-discharge treatment of propane–butane mixture in the ratio of 0.5:0.5. The structural characteristics of the synthesized materials are investigated through high-resolution electron microscopy and x-ray diffraction analysis. As revealed, the individual particles measured as of 20–40 nm in size assemble into agglomerates exhibiting a predominantly spherical morphology. Each particle is composed of multilayered, partially closed graphene shells with structural defects. As found, the synthesized material has graphite-like type of short-range atomic order. As shown, the addition of 10–20 wt.% of CNS into epoxy matrix results in increase of dielectric permittivity and shielding properties of composites in frequency range 26–40 GHz.

Досліджено вплив вуглецевих наносфер (ВНС) на електромагнетні властивості композитних матеріялів. ВНС одержували шляхом високочастотного електророзрядного оброблення пропан-бутанової суміші у співвідношенні 0,5:0,5. Структурні характеристики синтезованих матеріялів досліджено методами електронної мікроскопії високої роздільчої здат-

ности та рентґеноструктурної аналізи. Виявлено, що окремі частинки розмірами у 20–40 нм збираються в аґломерати, що мають переважно сферичну морфологію. Кожна частинка складається з багатошарових, частково замкнених графенових оболонок зі структурними дефектами. Встановлено, що синтезовані матеріяли характеризуються графітоподібним типом близького атомового порядку. Показано, що додавання 10–20 мас.% ВНС до епоксидної матриці приводить до підвищення діелектричної проникности й екранувальних властивостей композитів у діяпазоні частот 26–40 ГГц.

Key words: carbon nanospheres, permittivity, dielectric loss, electrical conductivity, electromagnetic shielding.

Ключові слова: вуглецеві наносфери, діелектрична проникність, електропровідність, діелектричні втрати, електромагнетне екранування.

(Received 29 November, 2024)

1. INTRODUCTION

The tremendous development of mobile communications, high-speed electronic switching components and circuits, radars, and systems of navigation operating in microwave range requires the effective protection of various electronic devices against the destructive impact of electromagnetic interference and ensuring electromagnetic compatibility. To solve this problem, the development of polymer composites filled with various nanoparticles is a perspective alternative way for efficient electromagnetic shielding [1, 2] compared with traditional metallic materials.

Among all the conductive nanofillers in polymer matrix, the nanocarbon is the most used as a component of polymer composites with carbon nanotubes, graphene, carbon black, carbon nanofibers and porous carbon due to the combined lightweight and remarkable mechanical, electrical and thermal properties as well as high corrosion resistance [3–5]. Nanocarbon fillers introduced in polymer matrix promote a significant increase in permittivity, and low dielectric loss at a low filler volume fraction, that is prospective for the development of high energy-density capacitors and electric field grading materials, owing to the unique property of dramatic increase in their dielectric constants near the percolation threshold [6, 7].

The observed enhancement in the permittivity can be attributed to the formation of a large network, which is composed of local microcapacitors with carbon particles as electrodes. Due to the high aspect ratio of nanocarbon fillers, carbon-based composites also exhibit enhanced microwave shielding properties and have demonstrated enhanced attenuation of electromagnetic radiation (EMR) due to the two

most important loss mechanisms, dielectric (dipolar) and conduction losses [8]. On the other hand, the good conductivity of carbon nanoparticles used as a microwave absorbing material has the shortcoming of poor impedance matching that results in high reflection of EMR on the first boundary 'air–composite'. To change the balance between the electromagnetic reflection and absorption into high microwave absorption capability of polymer-filled composite, some alternative ways are used, such as combining dielectric and magnetic fillers [9], the special microstructure design of composite [10], the development of uniform core–shell microstructures [11], carbon micro- and nanospheres [12, 13, 14], or carbon nanoonions (CNOs) particles [15, 16] that open up new perspectives for the creation the lightweight and highly efficient carbon-based microwave absorbing materials.

The special structure and high chemical activity of surface of the mentioned globular carbon particles, which are embedded in a polymer matrix results in the formation of a large number of active interfaces as centres for the multiple reflection and scattering of electromagnetic waves enhancing the microwave shielding–absorption capability of the composite. The electrical and electromagnetic properties of polymer composites filled with globular carbon particles significantly depend on the type, structure and morphology of carbon filler. For example, in Ref. [17], it was found that composites with content of mesoporous carbon hollow nanospheres (MCHS) lower than the percolation threshold possess excellent EMR absorbing behaviour, while composites with a MCHS content close to or higher than the percolation threshold reveal outstanding EM interference (EMI) shielding. Therefore, the EMR shielding effectiveness (SE) achieved an average value of 84.50 dB at MCHS content of 12 wt.%. On the other hand, for onion-like carbon (OLC)/polydimethylsiloxane composites with an average aggregate size of 250 nm, the percolation threshold was 10 vol.% and consequently, the electromagnetic shielding efficiency value is low [18].

This paper is focused on the synthesis of carbon nanomaterial by high-frequency electrical discharge treatment of hydrocarbon gases and study of their structural and morphology properties. In addition, we have prepared the epoxy composite materials (CMs) filled with synthesized nanocarbon materials—carbon nanospheres (CNS) to establish the influence of this type of nanocarbon filler on dielectric and shielding properties of two-phase CNS/epoxy CMs in a wide frequency ranges: 1–500 MHz and 26–40 GHz.

2. MATERIALS AND METHODS

2.1. Synthesis of Carbon Nanospheres

The studied carbon nanospheres were synthesized by high-frequency

electrical discharge treatment of propane–butane mixture ($C_3H_8 + C_4H_{10}$) in the ratio of 0.5:0.5. This technique was developed at the in the Institute for Pulse Research and Engineering of the National Academy of Sciences of Ukraine. The main idea is to create non-equilibrium electric discharge plasma due to the high frequency of passing short high-voltage pulses in the medium of gaseous hydrocarbons [19]. Providing high temperature and pressure gradients as necessary conditions for the synthesis of carbon nanomaterials is achieved through the high rate of energy input into the plasma channels. Non-equilibrium plasma, generated by discharges with a frequency of kilohertz, makes it possible to involve rather large volumes of gas in the synthesis process. In a reactor with special electrode systems, at atmospheric or slightly elevated pressure, the reaction products condense in the gas environment near the plasma channels. Visual observation showed that the reaction products condense in a gaseous medium at one or more centimetres from the plasma channel. Synthesis products were collected sometime after the equipment was turned off, allowing enough time for synthesis products to settle.

2.2. Composite Fabrication

The preparation of epoxy-filled composites was performed *via* ultrasonic dispersing of carbon nanospheres and epoxy resin (L285) mixture with subsequent curing in Teflon forms for complete polymerization. The preparation procedure was described in detail in Ref. [20]. The composite mixture is placed in an ultrasonic bath BAKU for dispersion during 2 hrs at power of 50 W. Ultrasound allows increase the homogeneity of filler particles distribution and to reduce the agglomeration of nanocarbon filler. After ultrasonic dispersing the curing agent H285 was added in the amount of 40% by the weight of the epoxy resin L285 and then the composite mixture was subjected to mechanical mixing. After that, the mixture was poured into suitable Teflon moulds. The polymerization took place at least 24 hrs at room temperature. After that, for the complete polymerization, the samples were treated at a temperature that gradually increased from 40 to 80°C for 5 hrs. After cooling the samples, they are ready for the measurements. The content of nanocarbon filler (CNS) was fixed at 10 and 20 wt.%. The samples are accordingly marked as xCNS/epoxy, where x is the weight content of CNS in the composite.

2.3. Methods

The structure of the synthesized carbon materials has been analysed

using high-resolution electron microscopy, XRD analysis, and the radial distribution function method. X-ray analysis was performed on a standard DRON-4 diffractometer with MoK_α monochromatic radiation in the Debye–Scherrer geometry. Electron microscopy was carried out on a JEOL JEM-2100F high-resolution electron microscope.

The study of the complex permittivity (ε_r', ε_r'') in the frequency range of 1–500 MHz was performed using Keysight Impedance Analyzer E4991B. The samples for the measurements were in the form of tablets with a diameter of 15 mm and a thickness of 1 mm. The shielding properties and complex permittivity spectra in the frequency range of 26.5–40 GHz were measured by Keysight PNA N5227A vector network analyser using the transmission–reflection method. The specimens were in the form of a plates with size 7.1×3.5×1.3 mm^3. The complex relative permittivity was derived from measured S-parameters (S_{ij}) of material using 85071 Agilent technology software [20].

Using S-parameters, the overall EMR shielding SE_T, shielding due to EMR reflection SE_R and absorption SE_A were determined [21]:

$$SE_R = 10\lg(1-|S_{11}|^2),\ SE_T = 10\lg(|S_{21}|^2),\ SE_A = SE_T - SE_R. \quad (1)$$

And the EMR reflection R, transmission T and absorption A indices are related to scattering parameters, respectively, as follow:

$$R = |S_{11}|^2,\ T = |S_{21}|^2,\ A = 1-|S_{11}|^2-|S_{21}|^2. \quad (2)$$

3. RESULTS AND DISCUSSION

3.1. Structure and Morphology of Synthesized Carbon Nanomaterials

High-resolution electron microscopy was used to determine the structure of individual particles. Figure 1 shows the typical micrographs of carbon nanospheres obtained by electric discharge treatment of propane–butane. It can be seen, that particles are collected into agglomerates (Fig. 1, *a*) and exhibit a globular shape with a size of ≅ 20–40 nm. It was also found that CNS have a complex hierarchical structure. The internal structure of a single particle consists of non-closed defective graphene layers (Fig. 1, *b*). This is typical of amorphous carbon.

Figure 2 represents typical XRD diffraction spectra from the crystalline graphite and obtained carbon nanospheres. The XRD spectrum for the sample synthesized by electric discharge treatment of gaseous hydrocarbon shows an intense broad peak at ≅ 11.1° coming from the (001) graphite crystal lattice plane (Fig. 2, *b*). This indicates that the material is characterized by an amorphous state and has a graphite-like

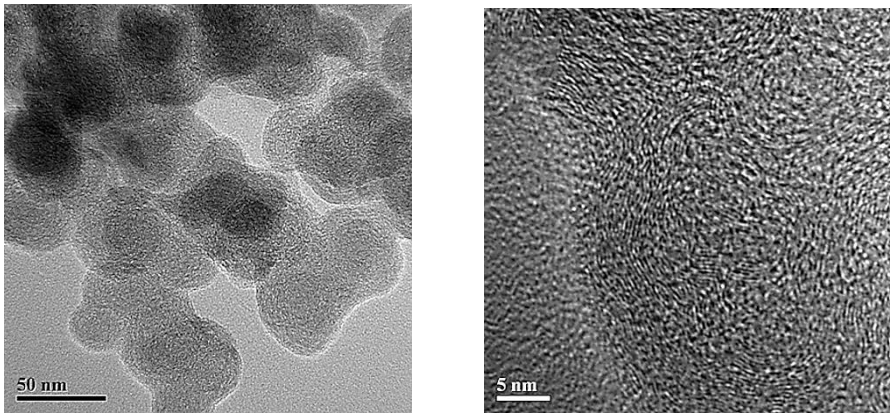

Fig. 1. High-resolution micrographs of carbon nanospheres obtained by electric discharge processing of propane–butane mixture.

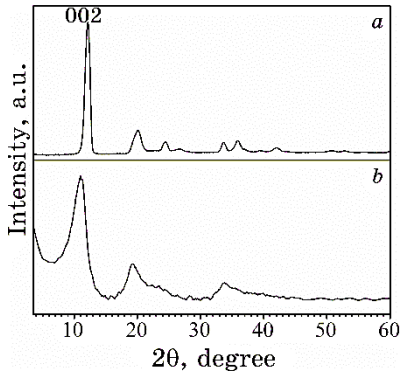

Fig. 2. Typical XRD patterns of graphite (*a*) and carbon nanospheres synthesized by electric discharge treatment of propane–butane mixture (*b*).

type of short-range atomic order. However, it should be noted that the maximum shifts to a smaller value 2θ relative to the position of the (002) peak of crystalline graphite (Fig. 2, *a*).

For a more detailed analysis of the material structure synthesized by electric discharge treatment of propane–butane mixture from XRD scattering intensities were calculated experimental structure factors (SF) and radial distribution functions (RDF) using the procedure described in Ref. [22]. The results of the calculated SF for the study samples are shown in Fig. 3, *a*.

On the SF of CNS, there is an intense peak with a maximum of $\sigma_1 = 1.74$ Å^{-1}, which corresponds to the graphite-like component. It confirms the conclusion that the obtained material possesses a

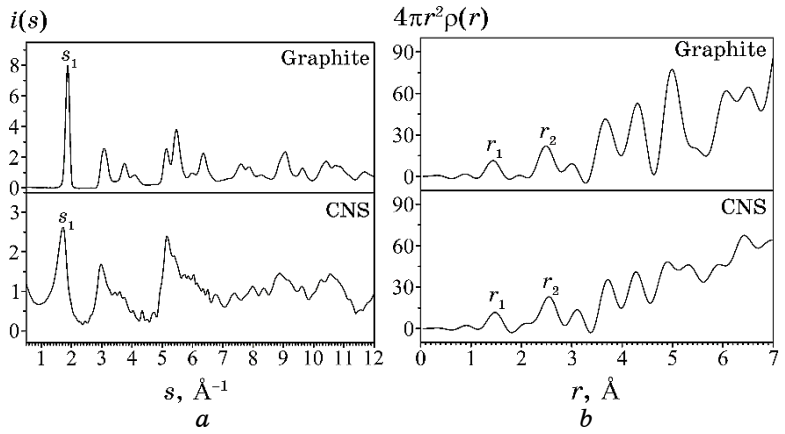

Fig. 3. Structure factors (*a*) and radial distribution function (*b*) of graphite and CNS.

graphite-like type of short-range atomic order. For crystalline graphite, the first peak has a position of $s_1 = 1.87$ Å^{-1}. By the width of the first maximum on the structure factor, using the formula given in Ref. [23], the size of ordering regions R_0 was determined. The calculation results obtained for all samples are presented in Table 1. It can be seen that the R_0 value for the CNS is of $\cong 38$ Å.

The first and second peaks in the radial distribution function of crystalline graphite are located at position of 1.43 and 2.48 Å, respectively. The positions of these peaks on the RDF for the synthesized CNS shift to higher values of 1.46 and 2.54 Å, respectively. A slight increase in the positions of the first and second co-ordination spheres indicates a partial disordering of the structure in comparison with that of crystalline graphite. The co-ordination number N_1 and bond angle Θ [22] are determined for samples from experimental RDF. The obtained data are represented in Table 1. The bond-angle Θ value for CNS is close to graphite (120°). However, the coordination number for them is much larger compared to graphite. Such an increase in the value of the coordination number may indicate that the CNS have a randomly close-packed structure.

3.2. Dielectric Properties of Epoxy Composites with Carbon Nanofiller

The complex permittivity ($\varepsilon_r^* = \varepsilon_r' - i\varepsilon_r''$) spectra of CNS–epoxy composites in the frequency range 1–500 MHz were determined using Impedance analyser E4991B. In the frequency range 26–40 GHz, permittivity spectra were derived from the measured *s*-parameters spectra using PNA N5227A vector network analyser. The results

are presented in Fig. 4.

As seen in Fig. 4, the adding CNS particle into epoxy matrix results in an increase in permittivity ε' up to the values of 8 and 17 (at 1 MHz) for 10 wt.% and 20 wt.% of CNS in composite, respectively. Such increase of permittivity is related to the electric nature of nanocarbon particles, acting as dipoles and enhanced interfacial polarization due to large difference between the electrical conductivity of filler and matrix phase and accumulation of charge carriers on 'nanocarbon–epoxy' interfaces. The observed gradual decrease of permittivity is explained by the relaxation of dipole polarization and stimulation of hopping (tunnel) conductivity with increasing EMR frequency. The imaginary part of permittivity ε_r'' is also increased with CNS content, especially for the microwave range 26–40 GHz that testifies the increase of A.C. conductivity of the composite. It should be noted that the permittivity values for the studied epoxy composites with 3*D* CNS nanoparticles (content 10 and 20 wt.%) are significantly lower compared with epoxy composites filled with 2*D* graphite nanoplatelets and 1*D* carbon nanotubes (content up to 5 wt.%). Such a difference in permittivity value may be explained by the high aspect ratio of GNP and CNT particles and agrees with Maxwell Garnett model predictions for the composites with carbon fibres [24, 25].

Since the ratio between the real and imaginary parts of permittivity is often more convenient for determining the nature of composite interaction with the electric field than the value of the imaginary part of the dielectric permittivity ε'', the dielectric-loss tangent $\tan\delta = \varepsilon''/\varepsilon'$ is used for the analysis of dielectric loss. Figure 4, *b* displays the dielectric-loss tangent $\tan\delta$ values for studied epoxy composites and as seen dielectric loss significantly increases with

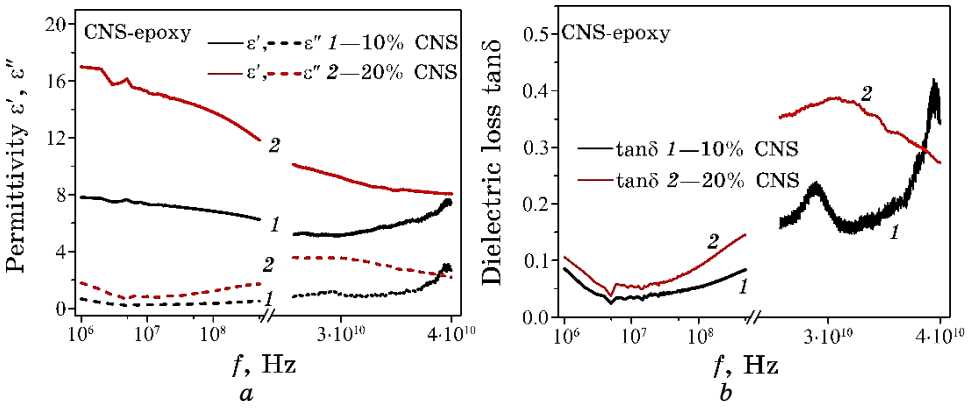

Fig. 4. Complex permittivity (*a*) and dielectric loss tangent (*b*) for CNS–epoxy CMs.

frequency, which is related to the increased conduction loss due to enhanced A.C. conductivity.

The conduction losses in composites occur from the electric leakage between electroconductive fillers and are described by the following equation [26]:

$$\varepsilon''_{rC} = \sigma_{D.C.}/(2\pi f \varepsilon_0)\,. \qquad (3)$$

Using the relation (3) the values of A.C. conductivity was calculated, and $\sigma_{A.C.}(f)$ dependences for the samples with 10 and 20 wt.% CNS are presented in Fig. 5.

As seen in this figure, the electrical conductivity increases with increasing frequency for all investigated frequency ranges. Such behaviour of A.C. conductivity $\sigma(f)$ can be described by an empirical Jonscher's power law, where the free term $\sigma_{D.C.}$ is the electrical conductivity at direct current [27]:

$$\sigma(f) = \sigma_{D.C.} + Af^u\,. \qquad (4)$$

The parameter A represents the strength of polarizability in the sample, whereas the parameter represents the reactivity between the sample constituent (such as the interaction between the fillers or the fillers with the polymeric chains).

In the case of studied CMs with 10 and 20 wt.% of CNS, the value of $\sigma_{D.C.}$ is low that results in a gradual increase of conductivity σ with f. The change in the A.C. electrical conductivity results from restructuring and reordering of charges at the sample's interface under an external electric field and interface polarization. As the frequency increas-

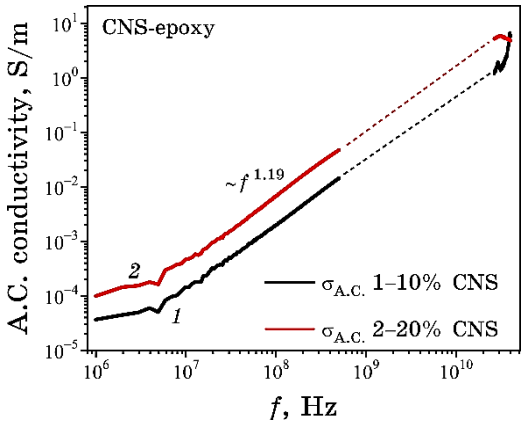

Fig. 5. A.C. conductivity of epoxy composites CNS/epoxy *versus* frequency with filler content 10 and 20 wt.%.

es, the capacitive resistance will decrease sharply, and some microcapacitors (formed by electrically conductive particles or clusters) become electrically conductive (activation of current carrier hopping (or tunnelling) increases), which leads to a decrease in permittivity and an increase in electrical conductivity. It was found that $\sigma(f) \propto f^{1.19}$, *i.e.*, exponent $u > 1$. Usually, exponent u lies in the range, and change $\sigma_{\text{A.C.}}$ with frequency is described within the correlated barrier hopping (CBH) model [28]. Such an increase of u exponent was also observed for PVA-treated MWCNT electrolyte composites [29] and testifies to a more complicated conduction mechanism in percolative nanocarbon-filled polymer composites.

3.3. Shielding Properties of Nanocarbon–Epoxy Composites

The development of polymer composite materials filled with electrically conductive carbon nanoparticles is the perspective way to achieve the excellent microwave shielding and absorption properties. The greater the number of charges (especially free current carriers) in the material, the higher is the level of EMR interaction with this material, and accordingly, the greater the EMR attenuation inside the sample.

The efficiency of the shield is determined by two main mechanisms: the reflection of part of the EMR from the front surface of the shield and the absorption of part of the EMR inside the shield material. Therefore, the total shielding efficiency of the material $SE_T = 10\log T$ is the sum of the term due to absorption SE_A and term due to reflection SE_R [30]:

$$SE_T = SE_R + SE_A. \tag{5}$$

The value SE_A characterizes the ability of the shield material to absorb the EMR that has transmitted inside the shield and the closer the ratio SE_A/SE_T to 1, the higher the absorption capability of the shield material. There is the following relation for the absorption term SE_A depending on the shield thickness l and the skin-depth δ_s ($\delta_s = 1/\sqrt{\pi f \mu \sigma}$) [31]:

$$SE_A = -8.7\, l/\delta_s = -8.7 l\alpha\,, \tag{6}$$

where α is the EMR attenuation index. The index $\alpha$and the skin-depth are determined by the electrodynamic parameters of the material—permittivity ε and permeability μ. Thus, the larger the shield thickness and the smaller the skin-depth the higher EMR shielding due to absorption. In addition, the presence of a large number of 'filler–polymer' interfaces in the composite promotes the high attenuation of

EMR due to effective processes of multiple reflection and electromagnetic wave scattering on these interfaces [32].

The shielding term due to reflection SE_R is determined by the impedance mismatch at the first boundary 'air–shield': the high impedance mismatch (as for metallic shields with high electrical conductivity) results in high EMR reflection index $|S_{11}|^2$ and enhanced SE_R shielding term.

The experimental results on the CNS/epoxy composites EMR shielding characteristics are presented in Fig. 6.

Figure 7 also presents the spectra of EMR reflection R, transmission T and absorption A indices for studied CNS/epoxy composites, which shows what part of incident electromagnetic radiation is reflected, absorbed inside the sample and transmitted through the shield.

As one can see in Fig. 6, the EMR shielding SE_T achieves the values 4–6 dB for 10 CNS/epoxy composite and increases with CNS content (20 wt.% CNS) up to the values 6–9 dB in the studied frequency range. Such an increase of SE_T values correlates with enhanced electrical conductivity due to a large number of added charge carriers. However, in epoxy CMs filled with 10–20 wt.% of CNS, the percolation threshold is not achieved, so D.C. electrical conductivity is low and shielding due to absorption (SE_A) is lower compared to the shielding due to reflection (SE_R), especially, for 10CNS/epoxy CNS (see Fig. 6, *b*). The decrease of EMR shielding $|SE_T|$ with frequency is explained by the dominating contribution of EMR reflection into total EMR shielding due to impedance mismatch at the first boundary 'air–composite sample'. As seen from Fig. 7, for studied composites at $f = 26.5$ GHz, EMR reflection index R is much higher (0.6–0.7) compared to EMR absorption index

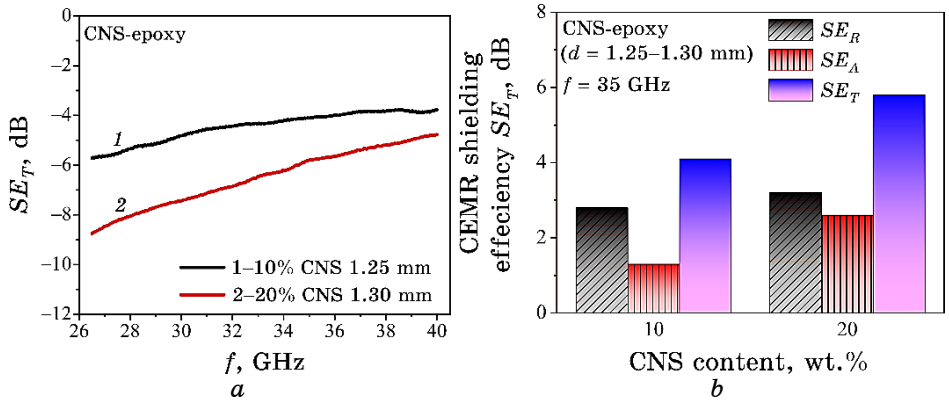

Fig. 6. Dependences of SE_T (*a*) on frequency and SE_T constituents on carbon nanospheres content in CNS/epoxy composites at 35 GHz (*b*). The thickness of the samples is of ≅ 1.3 mm.

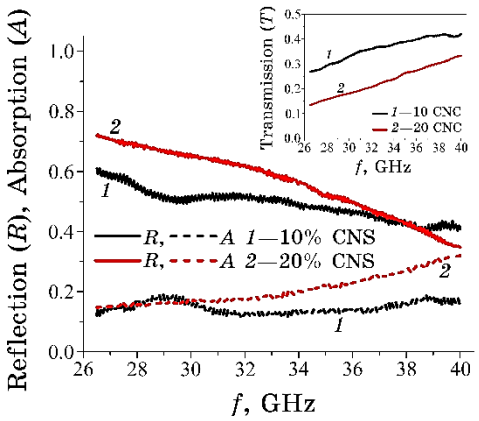

Fig. 7. EMR reflection, R transmission T and absorption A indices *versus* frequency for CNS/epoxy composites filled with 10 and 20 wt.% of CNS: solid line—reflection index, dashed line—absorption index and the inset displays EMR transmission index.

A (0.12) and decreases with frequency that results in a decrease in total shielding efficiency SE_T (increase of EMR transmission index T with f). The improvement of shielding and absorption capabilities of CNS-filled epoxy composites may be achieved via the increase of CNS content or combination of CNS filler with other conductive particles, such as 1D carbon nanotubes, 2D graphite nanoplatelets, or magnetic nanoparticles.

3. CONCLUSION

The effect of carbon nanomaterials, produced by high-frequency electrical discharge treatment of propane–butane mixture, on the electromagnetic properties of composite materials is established. It is revealed that individual particles represent carbon nanospheres (CNS) measuring 20–40 nm in size and assemble into agglomerates. Each particle is composed of multilayered, partially closed graphene shells with structural defects. The synthesized material has graphite-like type of short-range atomic order.

As shown, the addition of 10–20 wt.% of CNS into epoxy matrix results in an increase of complex dielectric permittivity $\varepsilon_r^* = \varepsilon_r' - i\varepsilon_r''$ that is related to the electric nature of nanocarbon particles, acting as dipoles and enhanced interfacial polarization due to the large difference between the electrical conductivity of filler and matrix phase. The observed increase of the imaginary part of permittivity ε_r'' with CNS content, especially, for the microwave range 26–40 GHz, testifies the increase of A.C. conductivity, which obeys the

empirical Jonscher's power law and increases due to the activation of current carrier hopping (or tunnelling) with frequency.

The electromagnetic shielding efficiency of CNS-filled epoxy composites SE_T increases compared to neat epoxy resin in the frequency range 26–40 GHz that correlates with enhanced electrical conductivity due to a large number of added charge carriers. The increase of CNS content up to 20 wt.% promotes the enhancement of EMR shielding due to absorption SE_A; however, the contribution to shielding due to reflection SE_R is still dominant in total EMR shielding efficiency.

This work was partially supported by project #8F-2024, which involved joint teams of scientists from Taras Shevchenko National University of Kyiv and the G. V. Kurdyumov Institute for Metal Physics of the N.A.S. of Ukraine.

REFERENCES

1. J. Guo, X. Li, Z. Chen, J. Zhu, X. Mai, R. Wei, K. Sun, H. Liu, Y. Chen, N. Naik, and Z. Guo, *J. Mater. Sci. Technol.*, **108**: 64 (2022); https://doi.org/10.1016/j.jmst.2021.08.049
2. Ján Kruželák, Andrea Kvasničáková, Klaudia Hložeková, and Ivan Hudec, *Nanoscale Advances.*, **3**, No. 1: 123 (2021); https://doi.org/10.1039/D0NA00760A
3. A. Kaushal and V. Singh, *J. Appl. Polym. Sci.*, **139**: e51444 (2022); https://doi.org/10.1002/app.51444
4. E. Mikinka and M. Siwak, *J. Mater. Sci: Mater. Electron.*, **32**: 24585 (2021); https://doi.org/10.1007/s10854-021-06900-8
5. M. Zhang, H. Ling, T. Wang, Y. Jiang, G. Song, W. Zhao, L. Zhao, T. Cheng, Y. Xie, Y. Guo, W. Zhao, L. Yuan, A. Meng, and Z. Li, *Nano-Micro Lett.*, **14**: 157 (2022); https://doi.org/10.1007/s40820-022-00900-x
6. R. Hashemi and G. J. Weng, *Carbon*, **96**: 474 (2016); https://doi.org/10.1016/j.carbon.2015.09.103
7. X. Xiong, H. Zhang, H. Lv, L. Yang, G. Liang, J. Zhang, Y. Lai, H.-W. Cheng, and R. Che, *Carbon*, **219**: 118834 (2024); https://doi.org/10.1016/j.carbon.2024.118834
8. R. Kumar, S. Sahoo, E. Joanni, R. K. Singh, W. K. Tan, K. K. Kar, and A. Matsuda, *Carbon*, **177**: 304 (2021); https://doi.org/10.1016/j.carbon.2021.02.091
9. B. Zhao, Y. Li, H. Ji, P. Bai, S. Wang, B. Fan, X. Guo, and R. Zhang, *Carbon*, **176**: 411 (2021); https://doi.org/10.1016/j.carbon.2021.01.136
10. G. Yang, M. Wang, J. Dong, F. Su, Y. Ji, C. Liu, and C. Shen, *Compos. B Eng.*, **246**: 110253 (2022); https://doi.org/10.1016/j.compositesb.2022.110253
11. Y. Zhao, H. Zhang, X. Yang, H. Huang, G. Zhao, T. Cong, X. Zuo, Z. Fan, S. Yang, and L. Pan, *Carbon*, **171**: 395 (2021); https://doi.org/10.1016/jcarbon.2020.09.036
12. Y. Song, F. Yin, C. Zhang, W. Guo, L. Han, and Y. Yuan, *Nano-Micro Lett.*,

13: 76 (2021); https://doi.org/10.1007/s40820-021-00601-x
13. Zhiqiang Lei, Yankang Wu, Liping Tang, and Jian Chen, *Polymer. Composite*, **43**, Iss. 11: 8181 (2022); https://doi.org/10.1002/pc.26986
14. M. Ghnimi, M. Mbarek, M. M. Almoneef,·H. Ghalla, and·K. Alimi, *Theor. Chem. Acc.*, **139**: 04 (2020); https://doi.org/10.1007/s00214-020-02619-7
15. F.-D. Han, B. Yao, and Yu-jun Bai, *J. Phys. Chem. C*, **115**: 8923 (2011); https://doi.org/10.1021/jp2007599
16. G. Siemiaszko, J. Breczko, A. Hryniewicka, A. Ilnicka, K. H. Markiewicz, A. P. Terzyk, and M. E. Plonska-Brzezinska, *Sci. Rep.*, **13**: 6606 (2023); https://doi.org/10.1038/s41598-023-33874-w
17. C. Wu, Y. Liu, and G. Zhao, *ACS Appl. Nano Mater.*, **7**, No. 8: 8926 (2024); https://doi.org/10.1021/acsanm.4c00438
18. J. Macutkevic, I. Kranauskaite, J. Banys, S. Moseenkov, V. Kuznetsov, and O. Shenderova, *J. Appl. Phys.*, **115**: 213702 (2014); https://doi.org/10.1063/1.4880995
19. L. Z. Boguslavskii, A. D. Rud', I. M. Kir'yan, N. S. Nazarova, and D. V. Vinnichenko, *Surf. Eng. Appl. Elect.*, **2**: 105 (2015); https://doi.org/10.3103/s1068375515020027
11. L. Vovchenko, O. Lozitsky, L. Matzui, V. Oliynyk, V. Zagorodnii, and M. Skoryk, *Mater. Chem. Phys.*, **240**: 122234 (2020); https://doi.org/10.1016/j.matchemphys.2019.122234
12. N. Abbas and H. T. Kim, *Macromol. Res.*, **24**: 1084 (2016); https://doi.org/10.1007/s13233-016-4152-z
13. J. Robertson, *Mater. Sci. Eng. R: Rep.*, **37**: 129 (2002); https://doi.org/10.1016/S0927-796X(02)00005-0
14. A. D. Alekseev, G. M. Zelinskaya, A. G. Ilinskii, I. G. Kaban, Yu. V. Lepeyeva, G. S. Mogilny, E. V. Ul'yanova, and A. P. Shpak, *Fiz. Tekh. Vys. Davl.*, **3**: 35 (2008).
15. L. Vovchenko et al., *Dielectric and Microwave Absorbing Properties of Epoxy Composites with Combined Fillers Nanocarbon/Inorganic Particles* (Eds. Z. Bartul and J. Trenor) (New York: Advances in Nanotechnology–Nova Science Publishers: 2023).
16. M. Y. Koledintseva, R. E. DuBroff, and R. Schwartz, *Progress in Electromagnetics Research*, **99**: 131 (2009); https://doi.org/10.2528/PIER09091605
17. W. Chao, H. Xingyi, W. Xinfeng, X. Liyuan, Y. Ke, and J. Pingkai, *Nanoscale*, **5**, No. 9: 3847 (2013); https://doi.org/10.1039/C3NR00625E
18. J. C. Dyre and T. B. Schroder, *Rev. Mod. Phys.*, **72**: 873 (2000); https://doi.org/10.1103/RevModPhys.72.873
19. S. R. Elliott, *Adv. Phys.*, **36**, No. 2: 135 (1987); doi:10.1080/00018738700101971
20. H. AlFannakh and S. S. Ibrahim, *J. Mater. Sci.: Mater. Electron.*, **33**: 24137 (2022); https://doi.org/10.1007/s10854-022-09092-x
21. R. Schulz, V. Plantz, and D. Brush, *IEEE Transactions on Electromagnetic Compatibility*, **30**, Iss. 3: 187 (1988); doi:10.1109/15.3297
22. Singh Kuldeep, Ohlan Anil, and S. K. Dhawan, *Nanocomposites—New Trends and Developments* (Ed. Farzad Ebrahimi) (InTechOpen: 2012), p. 15–33.
23. T. Shang, Q. Lu, J. Zhao, L. Chao, Y. Qin, N. Ren, Y. Yun, and G. Yun, *Nanomaterials*, **11**: 1444 (2021); https://doi.org/10.3390/nano11061444